THE STRUCTURE OF THE α_2-SUBUNIT OF THE F_1-ATPase FROM *ESCHERICHIA COLI* IN SOLUTION

Hasko H. PARADIES

Department of Chemistry, Cornell University, Ithaca, NY 14853, USA and *Fachrichtung Biochemie der Pflanzen, Freie Universität Berlin, Königin-Luise-Str. 12–16a, 1000 Berlin 33, Germany*

Received 4 November 1981; revision received 3 December 1981

1. Introduction

To gain structural information about the peripheral part of the H^+-translocating ATPase, F_1, from *Escherichia coli*, having a subunit composition of $\alpha_3\,\beta_3\,\gamma,\delta,\epsilon$ [1] which is compatible with small angle X-ray scattering experiments [1], the structures of the subunits of F_1 can be investigated and compared with the overall shape of the F_1 molecule [2]. I can now report the dimeric structure of α from F_1 in solution.

In [3–5] purified α- and β-subunits from TF_1 and F_1 in *E. coli* were both found to have nucleotide binding sites and it was claimed that the α-subunit had an allosteric site for TF_1 and that β carries the catalytic one. α from F_1-ATPase of *E. coli* carries a tight nucleotide site [5] with $K_d = 0.9\ \mu M$. The monomeric α-F_1 from *E. coli* changes its conformation upon binding to ATP [6–8]. This study shows that, under certain experimental conditions and in the absence of ATP and/or ADP and Mg^{2+}, α can be isolated as a dimer from which structural information of the protein–protein interaction (α–α) can be obtained.

2. Materials and methods

2.1. *Preparation of α-subunit and α_2*

The α-subunit was prepared according to [5] and further purified by high-pressure liquid chromatography on an I 120 column from Waters, Associates, applying a flow rate of 2.5 ml/min and an elution buffer consisting of 0.05 M Tris–PO_4 (pH 8.0), 0.1 mM EDTA and 0.1 mM dithiothreitol. The purified α-subunit was dialyzed against 0.05 M K_2HPO_4 (pH 6.5) at 4°C, at 2 mg protein/ml for 12 h in the presence of 10% (v/v) glycerol.

Formation of α_2-F_1-ATPase was achieved by heating the dialyzed solution of α at pH 6.5 in the presence of 10% (v/v) glycerol and 1 mM Mg^{2+} to 37°C for 30 min. Chromatography on an I 250 column by high-pressure liquid chromatography at 2.5 ml/min, using a buffer system for elution consisting of 0.05 M K_2HPO_4 (pH 6.5), containing 1 mM dithiothreitol, 1 mM Mg^{2+} and 10% (v/v) glycerol, shows a major peak, equivalent to 130 000 M_r after calibration of the column with proteins of known hydrodynamic properties, and a minor peak, only 5% of the total initial loading of the column, representing α-monomeric.

The purity of α_2 was 98%, as proven by polyacrylamide gel electrophoresis [5], revealing no contamination of proteins of low M_r. The homodispersity of α_2 was proven by analytical ultracentrifugation [10] and inelastic light scattering [6]. The protein concentration was determined spectrophotometrically at 278 mm using an extinction coefficient of $A^{0.1\%,\,1\ cm}_{278\ nm} = 0.51$, determined by interferometric methods [11].

2.2. *Small angle X-ray scattering*

The measurements were carried out as described extensively in [2,8], using a G X 18 rotating anode (Elliot, UK) with a Cu-target, operated at 45 kV and 30 mA. Protein solutions were investigated at 20°C and 4°C. Each scattering curve, which was recorded on a one-dimensional position-sensitive detector system (Tennelec, Oak Ridge TN), was measured several times with a fixed number of counts of 10^5/angle to minimize statistical errors [12]. The procedure used for data evaluation and processing, as well as density

Abbreviations: F_1, the peripheral part of the H^+-translocating ATPase (EC 3.6.1.3) from *E. coli*; $\alpha,\beta,\gamma,\delta$ and ϵ, subunits of F_1 in order of decreasing M_r-value

Published by Elsevier Biomedical Press
00145793/82/0000–0000/$02.75

measurements for the partial specific volume of α_2 is described in [13].

Model calculations of the random-orientated α_2 molecule in solution show that the particle can be assumed to be an assembly of n hard spheres each with a radius of 0.5 nm. In order to evaluate the scattered intensity curves for α_2 and to compare them with possible molecular models, the Debye formula was used according to equation:

$$I(h) = \sum_i \sum_k f_i f_k \frac{\sin hR_{ik}}{hR_{ik}} \quad (1)$$

with f_i and f_k the scattering amplitudes of atoms or nuclei situated at points i and k, respectively, and R_{ik} is the distance between the nuclei [14]. In a further approximation the particle under consideration, α_2, was constructed from a number of homogeneous identical hard spheres (radius 0.5 nm). Modifying eq. (1), the normalized scattered intensity, $I_n(h) = I(h)/I(h = O)$ can be calculating according to:

$$I_n(h) = \frac{9\pi}{2}\left[-\frac{J\,3/2\,(hR)}{hR^3}\right]^2 \times \left[\frac{n + 2\sum_{j=1}^{m} A_j \sin\frac{hR_j}{hR_j}}{n^2}\right] \quad (2)$$

with J the Bessel function, equivalent to the scattering intensity curve of a sphere with radius R; n is the number of spheres filling the particle (α_2), A_j represents the number of distances $R_{ik} = R_j$, and n is the number of different distances R_j [14]. Calculations were performed on the Cornell computer IBM 3700 and the MSC 400 primer computer.

3. Results

From the innermost portion of the scattering curve according to [15] the apparent radius of gyration was obtained (fig.1), which was extrapolated to

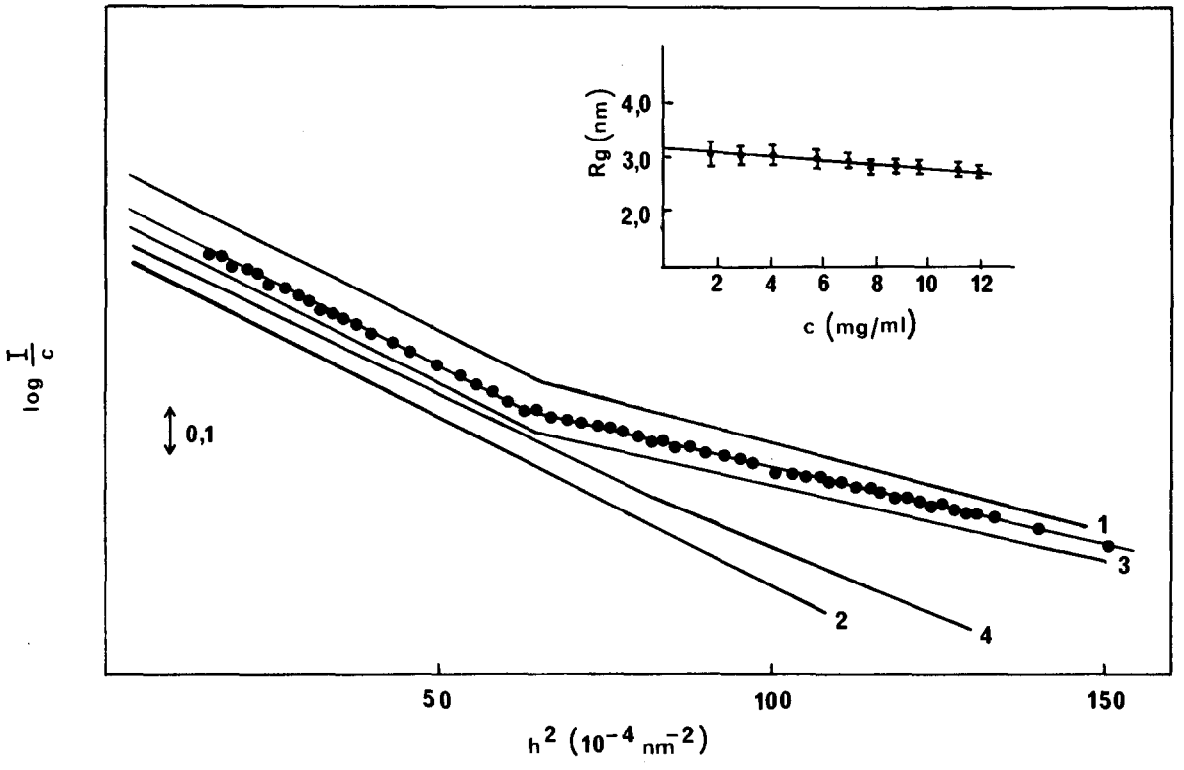

Fig.1. X-Ray scattering of α_2 in 0.05 M K_2HPO_4, containing 1 mM dithiothreitol, 1 mM Mg^{2+} and 10% (v/v) glycerol, at pH 6.5, in a Guinier plot. I is the scattered intensity and c the concentration of the protein in mg/ml. Inset: concentration dependence of the radius of gyration; (——) calculated intensity distribution for model 3 of fig.4.

vanishing protein concentration. High precision values for R_g were obtained by evaluation of the radius of gyration from the distance distribution function, $D(R)$, using data from the entire scattering curve according to:

$$R_g^2 = \frac{\int_0^D D(R)R^2 dR}{2\int_0^D D(R)dR} = \frac{\int_0^\infty H(x)x^4 dx}{2\int_0^\infty H(x)x^2 dx} \quad (3)$$

with $H(x)$ the correlation function:

$$H(x) = (1/2\pi^2) \times \int_0^\infty KI(h)h^2 \left[\sin\frac{(hx)}{(hx)}\right] dh$$

where K is a constant [16,17]. Since the Guinier approximation holds only for a limited angle range, $R_g = 3.09 \pm 0.07$ nm at 20°C and $R_g = 3.06 \pm 0.05$ nm at 4°C were obtained when taking the entire scattering function for α_2 into consideration according to eq. (3). Whereas R_g from the Guinier region can be approximated with an accuracy of better than 9.5% in the range of $hR < 0.9$, an accuracy better than 1% (hR_g) is obtained by collecting data down to 0.4 and applying the correlation function [13]. During the measurements of α_2 at pH 6.5 no significant dissociation or association were detected. The M_r-value was determined by extrapolation to zero scattering angle, where the experimental intensity was put on an absolute scale by means of calibrated Ni-filters (Dupont, DL) according to [2]. An M_r of 105 000 ± 10 000 for α_2 at pH 6.5 was obtained, applying an isopotential partial specific volume of $\phi = 0.738 \pm 0.002$ ml/g, obtained by densitometry measurements [13]. The largest expansion of α_2 can be obtained by the distance distribution function, $D(R)$, directly from the scattered intensity (fig.2). The relative weakness of the oscillations and the negligible concentration effects led us to conclude that the scattering pattern in all measured points was not significantly distorted, including the termination effects of the Fourier transformation [16]. This is consistent with the observed findings that the scattering pattern at wider angles does not change significantly over a mode range of α_2 concentration. Once $D(R)$ and D_{max} have been calculated (table 1), the zero scattering intensity, $I(0,\rho_0) = 4\pi\int_0^\infty D(R)$, can give additional information about the M_r-value which, applying the whole set of scattering data [16], was evaluated to 115 000 (table 1).

From the distribution of the scattered intensity

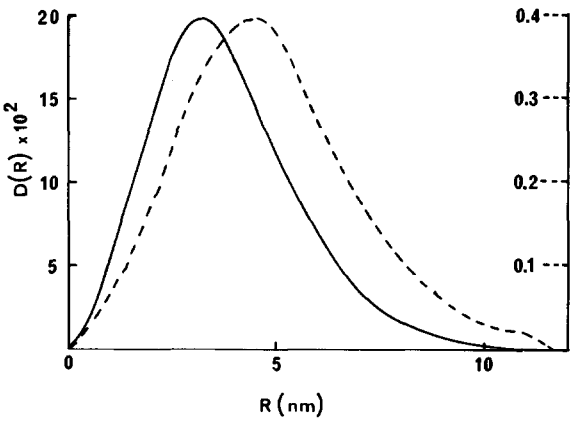

Fig.2. Distance distribution function of α_2 (——) and of the F_1-ATPase ($\alpha,\beta,\gamma,\delta,\varepsilon$) (– – –) for comparison.

it is possible to determine the distribution of chords, i.e., the distribution of the length of the straight segments joining 2 points on the external surface of the particle [18,19], calculated according to Tschoubar as in [20]. The distribution of chords is shown in fig.2, revealing that the maximum dimension is 11.0 nm, the same as was obtained from $D(R)$, and it should be noticed that the value of $G(R)$ for $R = 0$ does not go to zero. Since the scattered intensity, which has been recorded up to an angle corresponding to $H = 0.31$ nm^{-1}, and the product of $I(h) \times h^4$ could be recorded with confidence, the volume of the particle could be determined. The volume of α_2 was found to be 2.4×10^3 nm^3 ± 5%, according to this method. The electron density contrast between hydrated α_2 and buffer if 91 e/nm^3. The degree of hydration of α_2 corresponds to 0.21 g water/g protein, and the ratio of surface to volume is 25% lower for α_2 than for α, alone [8].

4. Discussion and conclusion

The size and shape of a particle or particle assembly can be characterized by 3 parameters: radius of gyration; volume; and external surface area. Since the maximum enlargement of the particle under consideration is determined from the distance distribution function, $D(R)$, as well as from $G(R)$ (fig.3), a fourth parameter can define the length of a and b of the semiaxis of a possible ellipsoid of revolution [21] (table 1). The values involving the surface area of α_2

Table 1
Structural parameters for α_2 from small angle X-ray scattering experiments

Parameter	Unit	Value
R_g	nm	3.09 ± 0.07
R_{c_1}	nm	2.70 ± 0.05
R_{c_2}	nn	1.35 ± 0.05
$M_r \times 10^4$		10.5 ± 1.0
$V \times 10^2$	nm^3	2.45
S_{ext}	nm^2	1.34 × 10^2
ϕ	ml/g	0.738 ± 0.002
R	nm	4.16
R_V	nm	3.98
R_S	nm	4.15
D_{max}	nm	11.0 ± 0.8
ω	g H_2O/g protein	0.39
$\frac{3V}{R_g^3}[2 + (a/b)^2]^{1/3}$	axial ratio	4.1
$S_{ext}/V\,[2 + (a/b)^2]^{1/3}$	axial ratio	4.4

R, R_V and R_S are the radii of spheres whose radii of gyration, of volume and of surface are R_g, V and S, respectively; deviations of these radii are indications of a departure from a spherical molecule

R_c is the radius of gyration of the cross-section, obtained from a plot of log $I(h) \times h$ vs h^2

correspond to more anisometric ellipsoids than those calculated from the determined volume, which can be explained by the surface roughness of α_2. The calculation of equivalent ellipsoids leads to a model of a prolate ellipsoid of revolution with an axial ratio of 4, as determined by V and R_g and from $D(R)$ and $G(R)$. The maximum enlargement of the dimer of α was found to be 11.0 ± 1.0 nm and from the distribution of chords ($G(R)$) it was found to be 9.5 ± 1.0 nm. However, the fact that the function $G(R)$ does not take the value of zero at $R = 0$ is explained by the presence of a large cleft, probably related to the impinging of the 2 ellipsoids of α.

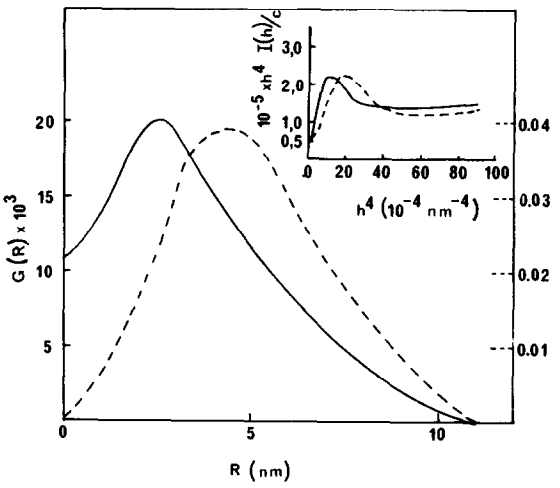

Fig.3. Distribution of chords ($G(R)$) of α_2 (——). Inset: the function of $i(h)ch^4$ plotted vs h^4 for α_2 (——) and for the F_2-ATPase (– – –).

Similar to the distribution of the scattered intensity at low scattering angles (fig.1), the distribution of the scattered intensity, represented as a cross-section plot, is characterized by 2 straight-line portions with 2 values of the radii of gyration of the cross-section (fig.4; table 1), namely, R_{c1} = 1.70 nm and R_{c2} = 1.35 nm. Model calculations according to eq. (2), built of 298 spheres, yield a radius of gyration very similar to the experimental value, when using model 1; however, the radii of gyration of the cross-section have a much lower value than the experimental one. A rod-shaped model (model 2) with 2 α-molecules joined together, having the same cross-section, is somewhat longer than the one determined from the pair distribution function of 11.0 nm. Furthermore, the radius of gyration is 10% higher. However, the third model in fig.4 fits the experimental curve reasonably well, as well as that of the calculated Guinier plot. The end-to-end distance of model 4 is 11.5 nm

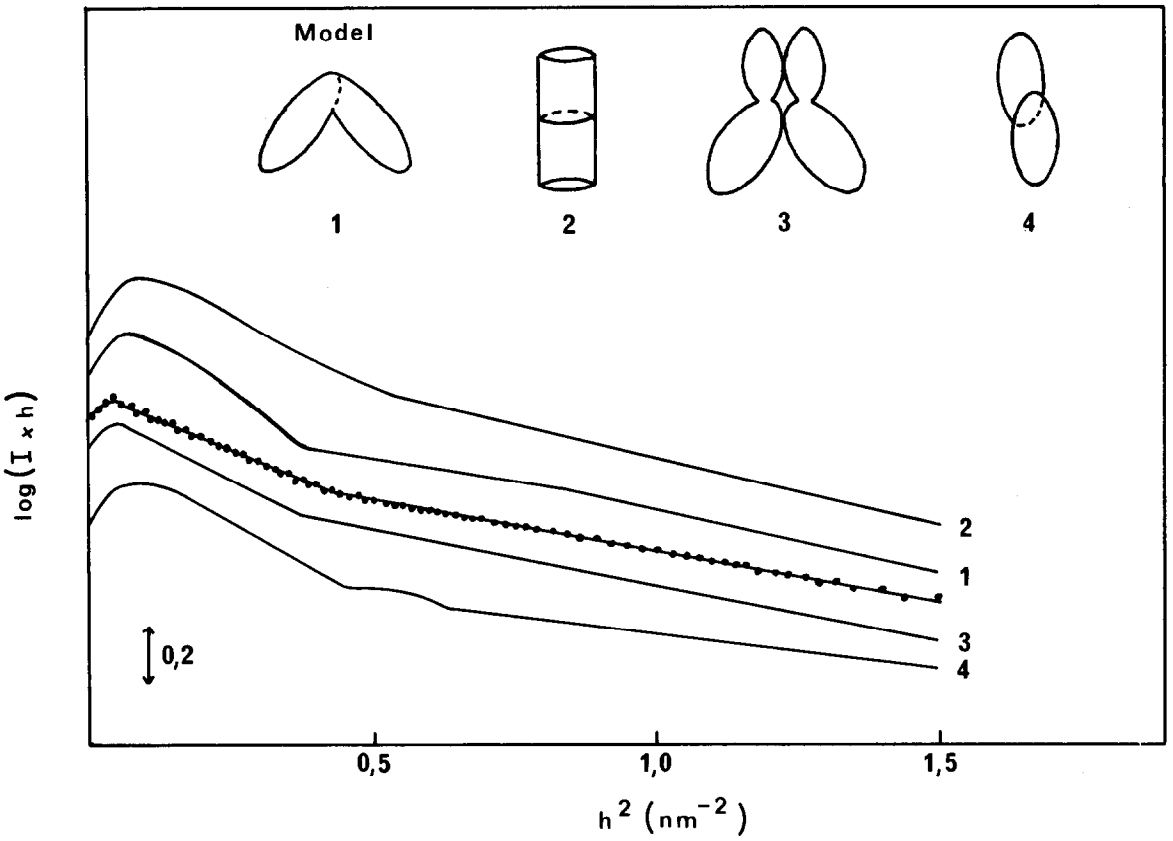

Fig.4. Calculated cross-section plots (——) of models 1–4 of α_2. Numbers correspond to model numbering in the inset. Experimental (. . .) data points. The straight lines were approximated by the steep and flat parts of the scattering curve using a weighted least squares routine.

which is in fair agreement with the experimental value. This is also the case for the calculated radius of gyration, which was calculated to 3.10 nm, and for the radius of gyration of the cross-section (R_{c1} = 2.70, R_{c2} = 1.40 nm). Similar to model 3, model 4 does not fulfil the radius of gyration, although it fits the radius of gyration of the cross section. Furthermore, it was observed that the radius of gyration of cross-section R_{c2} depends mainly on the thickness of the α-subunit, when fitting experimental data to models. When the thickness was decreased, the outer part of the cross-section curve at higher scattering angles became more steep. The slope of the inner part of the calculated cross-section curve, which is proportional to R_{c1}^2, reveals a different dependence on the thickness of the α-subunit, namely it decreases. These dependencies apparently indicate that R_{c1} and R_{c2} are not real cross-section radii of rod-like structures, but characteristics of the α-scattering curves.

In comparison to the native enzyme, the F_1-ATPase, we note some similarities:

(1) The radius of gyration is large when compared to a hard-sphere, multisubunit particle; the ratios of the cubes of the radii of gyration are almost twice the ratio of the volumes, indicating that the dimeric structure of α_2 is more anisometric than F_1, which is a hollow sphere [2].

(2) The distribution of the scattered intensity near the origin appears to be bimodal since the Guinier plot (fig.1) displays 2 linear regions with an abrupt change at $h = 7.07 \times 10^{-2}$ nm^{-1}. Similar results were discovered for the entire F_1-ATPase from *E. coli* [2]; however, there the change appeared at $h = 8.6 \times 10^{-2}$ nm^{-1}. This bimodal distribution suggests the presence of at least 2 parts loosely connected together.

(3) The distribution of chords, $G(R)$ (fig.3), reveals a rather slow fall off at large R. This can be

explained by an association of ⩾2 globular parts, linked together by a fairly flexible hinge. In contrast to the F_1-ATPase, where $G(R)$ does go to zero at $R = 0$, α_2 has a finite value beyond zero, supporting the idea of localizing the flexible hinge in α. This is further substantiated by the fact that the flexible hinge and the change of $G(R)$ at $R = 0$, displayed in fig.3, is abolished when treating α_2 with trypsin.

Furthermore, the ability of binding ATP to α_T is abolished [22]. Moreover, proteolysis of α of M_r = 55 700 [8] occurs through cleavage at the amino-terminal end of α, resulting in 2 fragments, one with 15 amino acid residues and a larger one of M_r 48 500 (α_T) [23]. In view of the dimeric structure of α under the studied conditions it is likely that these particular distinct parts of α or α_2 are related to the observed flexible hinge. This strongly suggests that the 2 monomers of α and the 3 α within the F_1-ATPase are linked together, essentially through interactions involving the NH_2-terminal extremity of each subunit. Fluorescence depolarization lifetime experiments on α of the F_1-ATPase from the thermophilic bacterium PS3 revealed a high degree of flexibility which is abolished upon binding of ATP [24], very similar to α from *E. coli* F_1-ATPase described here.

Acknowledgements

The author thanks Dr M. Leonowicz for providing computer facilities and Dr E. Kramer for providing small angle X-ray scattering facilities.

References

[1] Fillingame, R. H. (1980) Annu. Rev. Biochem. 49, 1079–1113.
[2] Paradies, H. H. and Schmidt, U. D. (1979) J. Biol. Chem. 254, 5257–5263.
[3] Yoshida, M., Sone, N., Hirata, H. and Kagawa, Y. (1977) Proc. Natl. Acad. Sci. USA 74, 936–940.
[4] Ohta, S., Tsubai, M., Oshima, T., Yoshida, M. and Kagawa, Y. (1980) Biochem. J. (Tokyo) 87, 1609–1617.
[5] Dunn, S. D. (1980) J. Biol. Chem. 255, 11857–11860.
[6] Paradies, H. H. (1980) FEBS Lett. 120, 289–292.
[7] Dunn, S. D. and Futai, M. (1980) J. Biol. Chem. 255, 113–118.
[8] Paradies, H. H. (1981) Eur. J. Biochem. 118, 187–194.
[9] Paradies, H. H. and Vettermann, W. (1979) Arch. Biochem. Biophys. 194, 88–100.
[10] Paradies, H. H. and Franz, A. (1976) Eur. J. Biochem. 67, 23–29.
[11] Paradies, H. H. (1979) J. Biol. Chem. 254, 7495–7504.
[12] Berington, P. R. (1969) Data Reduction and Error Analysis for the Physical Sciences, McGraw Hill, New York.
[13] Paradies, H. H. (1980) J. Phys. Chem. 84, 599–607.
[14] Guinier, A. and Fournet, J. G. (1955) Small-Angle Scattering of X-Rays, Wiley, New York.
[15] Guinier, A. (1939) Ann. Physik. 12, 161–237.
[16] Glatter, O. (1979) J. Appl. Crystallog. 12, 166–175.
[17] Müller, K., Laggner, P., Glatter, O. and Wostner, G. (1978) Eur. J. Biochem. 82, 73–90.
[18] Tschoubar, D. and Mering, J. (1969) J. Appl. Crystallog. 2, 128–138.
[19] Luzzati, V., Tardieu, A., Mateu, L. and Stuhrmann, H. B. (1976) J. Mol. Biol. 101, 115–127.
[20] Paradies, H. H., Schmidt, U. D. and Zimmermann, J. (1978) J. Biol. Chem. 253, 8972–8979.
[21] Scheraga, H. A. (1961) in: Protein Structure (Kaplan, N. O. and Scheraga, H. A. eds) pp. 2–18, Academic Press, New York.
[22] Dunn, S. D., Heppel, L. A. and Fullmer, C. S. (1980) J. Biol. Chem. 255, 6891–6896.
[23] Dunn, S. D. and Heppel, L. A. (1981) Arch. Biochem. Biophys. 210, 421–436.
[24] Paradies, H. H. and Kagawa, Y. (1981) FEBS Lett. 136, 3–7.